

Article

Second Law Analysis of Dissipative Flow over a Riga Plate with Non-Linear Rosseland Thermal Radiation and Variable Transport Properties

Muhammad Idrees Afridi ¹, Muhammad Qasim ¹ and Abid Hussanan ^{2,3,*} 

¹ Department of Mathematics, COMSATS Institute of Information Technology, Park Road, Chak Shahzad, Islamabad 44000, Pakistan; idreesafridi313@gmail.com (M.I.A.); mq_qau@yahoo.com (M.Q.)

² Division of Computational Mathematics and Engineering, Institute for Computational Science, Ton Duc Thang University, Ho Chi Minh City 700000, Vietnam

³ Faculty of Mathematics and Statistics, Ton Duc Thang University, Ho Chi Minh City 700000, Vietnam

* Correspondence: abidhussanan@tdt.edu.vn

Received: 17 July 2018; Accepted: 15 August 2018; Published: 18 August 2018



Abstract: In this article, we investigated entropy generation and heat transfer analysis in a viscous flow induced by a horizontally moving Riga plate in the presence of strong suction. The viscosity and thermal conductivity of the fluid are taken to be temperature dependent. The frictional heating function and non-linear radiation terms are also incorporated in the entropy generation and energy equation. The partial differential equations which model the flow are converted into dimensionless form by using proper transformations. Further, the dimensionless equations are reduced by imposing the conditions of strong suction. Numerical solutions are obtained using MATLAB boundary value solver bvp4c and used to evaluate the entropy generation number. The influences of physical flow parameters arise in the mathematical modeling are demonstrated through various graphs. The analysis reveals that velocity decays whereas entropy generation increases with rising values of variable viscosity parameter. Furthermore, entropy generation decays with increasing variable thermal conductivity parameter.

Keywords: entropy generation; heat transfer; variable transport properties; Riga plate; viscous and magnetic dissipation; non-linear Rosseland thermal radiations

1. Introduction

In the classical MHD flow control, the boundary layer flow of an electrically conducting fluid can be controlled by the application of an external magnetic field subjected to the condition that the electric conductivity of fluid should be high (e.g., liquid form of semiconductors, plasma, electrolytes and liquid metals). Due to the high electric conductivity of the fluid, the influence of applied external magnetic field is significant even in presence of moderate strength of the magnetic field (~1 Tesla). In addition, the application of an external electric field is not required in order to achieve an efficient flow control. In case of weakly conducting fluids (e.g., sea water) the electric current induced by the external magnetic field is too small and external electric field must be applied to control the flow separation. The Lorentz force parallel to the wall has the ability to stabilize the motion inside the boundary layer by slowing down its growth. Gailitis and Lielausis [1] proposed for the first time an ingenious way to produce the wall-parallel Lorentz force. The flow control device developed by Gailitis and Lielausis [1] consists of alternative permanent magnetics and electrodes of equal width. Later on, Avilov [2] called it the Riga plate [2]. Perhaps, for the very first time, Tsinober and Shtern [3] used the Grinberg-term in the momentum equation to analyze the boundary layer flow.

The Grinberg-term is free from flow velocity and decays exponentially with the distance normal to the main flow. The influence of suction/injection on classical Blasius and Sakiadis flow over a Riga plate is investigated by Pantokratoras [4]. Magyari and Pantokratoras [5] reported the mixed convection flow of Newtonian fluid induced by the Riga plate. Ahmed et al. [6] employed the perturbation technique and numerical simulation to study the mixed convection flow of nanofluid past over a Riga plate. The effects of non-linear thermal radiation on the Blasius and Sakiadis flow of nanofluids over a Riga plate by taking the effects of Brownian diffusion and thermophoresis is studied by Ramesh and Gireesha [7]. Pantokratoras and Magyari [8] numerically investigated the free convection flow over a Riga plate by using the tridiagonal matrix algorithm.

The non-linear thermal radiation has major importance in the high-temperature processes. The linear thermal radiation approximation is valid in the low-temperature processes. The effects of non-linear Rosseland thermal radiation on the classical Sakiadis and Blasius flows are investigated by Pantokratoras and Fang [9,10]. Recently, Afridi and Qasim [11] reported the influences of non-linear thermal radiation on heat transfer and entropy production in a fluid flow over a horizontally moving thin needle. Sithole et al. [12] examined the viscous dissipation and non-linear radiation impacts on the entropy generation rate in a second grade nanofluid flow over an elastic stretching sheet. The effects of variable viscosity and nonlinear thermal radiation on bio-convection flow by taking gyrotactic microorganisms in the presence of Lorentz force are reported by Babu and Sandeep [13]. Very recently Ghadikolaei et al. [14] studied the Casson fluid flow over a permeable inclined stretching surface by incorporated the influence of magnetic field.

In the case of high-temperature processes, it is more convincing to consider the viscosity and thermal conductivity to be temperature dependent. The influence of temperature dependent viscosity on mixed convection flow is reported by Hossain and Munir [15]. Khader and Megahed [16] performed the first law analysis of viscous fluid flow over a slendring stretching surface by taking the temperature-dependent thermal conductivity and linear thermal radiation. Mureithi et al. [17] found that the variable viscosity parameter has substantial impacts on temperature and velocity distribution inside the boundary layer. The combined effects of variable thermal conductivity and variable viscosity on a mixed convection flow under the impact of Lorentz force is investigated by Pal and Mondal [18]. Their investigation reveals that temperature profile enhances with enhancing values of variable thermal conductivity parameter. Manjunatha and Gireesha [19] studied dusty fluid flow with variable viscosity and thermal conductivity under the influence of magnetic force.

From an industrial point of view, the analysis of heat transfer in boundary layer flows is of great importance [20–22]. In the recent past, the heat transfer analyses in industrial processes involving either closed or open system are confined to first law analysis. The main purpose of the first law analysis is to find the temperature distribution inside the thermodynamic system and the rate of heat flux at the solid boundary [23–25]. This is a well-known fact that in all real thermodynamic processes the quantity of energy is conserved but the quality of energy reduces [26]. The reduction in quality of energy in thermodynamic processes is measured by entropy generation. In other words, the quality of energy decays with the enhancement of entropy generation in a process. There are many causes of entropy generation such as fluid friction, mixing, dissipative forces, heat transfer and unrestrained expansion etc. The aim of the second law analysis is to minimize the entropy generation in a thermodynamic system. Bejan [27] pulled out the way to reduce the entropy generation in a convective heat transfer problem and called it entropy generation minimization (EGM). After the innovative work of Bejan [27], many researchers used the second law of thermodynamics to minimize the entropy generation. Some of the recent studies on the second law analysis are referenced in [28–35].

The aim of the present study is to investigate the flow and heat transfer analysis of the dissipative flow induced by a horizontally moving Riga plate in a quiescent fluid with variable transport properties and non-linear Rosseland thermal radiations. The second law analysis is also performed in the presence of viscous dissipation. The governing equations are non-dimensionalized with the help of suitable transformations. The dimensionless equations are further simplified by using the assumption of strong

suction. The reduced set of governing equations is solved numerically by utilizing MATLAB built-in boundary value solver bvp4c. The variations of quantities of interests with emerging dimensionless numbers are portrayed graphically and discussed physically in detail. To the best of author’s knowledge, such an analysis is not reported before.

2. The Mathematical Model

An incompressible boundary layer flow over a Riga plate moving horizontally in a quiescent electrically conducting fluid is considered. The temperature of the ambient fluid and the velocity of Riga plate are assumed to be constant and denoted by T_b^* and u_w^* , respectively. The thermal conductivity and viscosity of the fluid are assumed to be temperature dependent. Figure 1a,b respectively show the Riga plate (also known as an electromagnetic actuator) which consists of permanent magnets and electrodes of equal width a_0 and sketch of the velocity and temperature profile. In addition, the temperature of the surface of Riga plate T_w^* is supposed to be constant such that $T_w^* > T_b^*$ (heated Riga Plate). Based upon the above flow assumptions, the governing equations in the presence of non-linear thermal radiation and viscous dissipation take the following form:

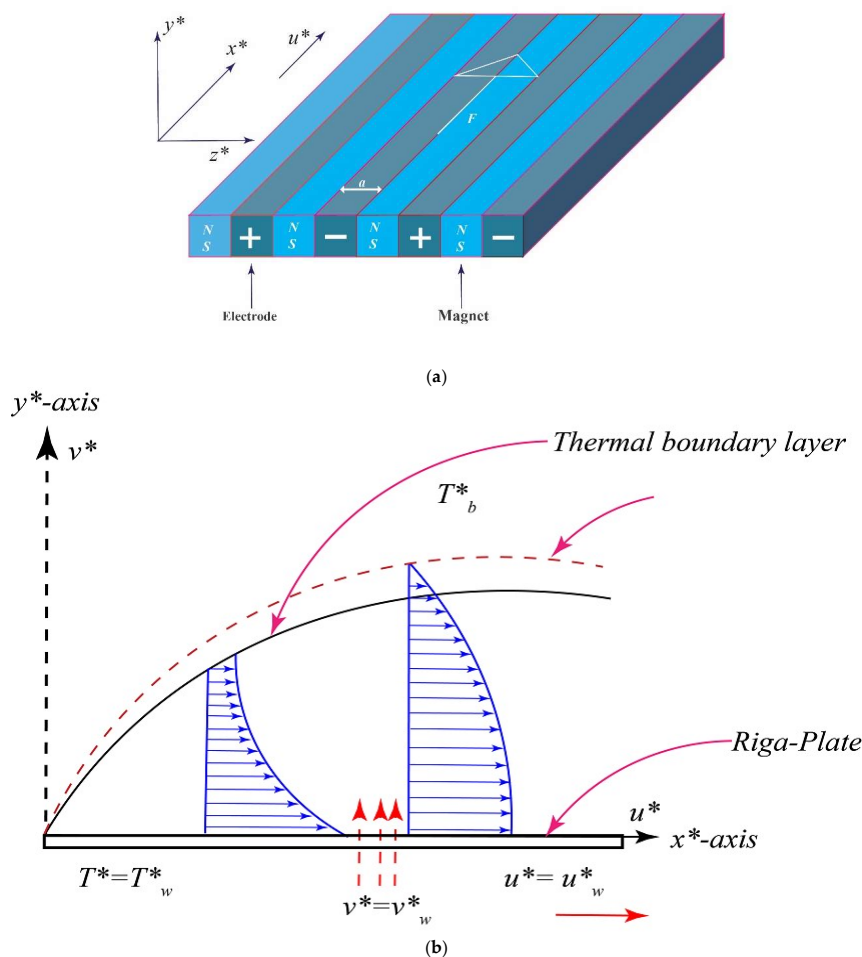


Figure 1. (a) Sketch of Riga plate with coordinates system; (b) Sketch of the flow showing the velocity and temperature profile.

$$\frac{\partial u^*}{\partial x^*} + \frac{\partial v^*}{\partial y^*} = 0, \tag{1}$$

$$\rho \left(u^* \frac{\partial u^*}{\partial x^*} + v^* \frac{\partial u^*}{\partial y^*} \right) = \frac{\partial \mu(T^*)}{\partial T^*} \frac{\partial T^*}{\partial y^*} \frac{\partial u^*}{\partial y^*} + \mu(T^*) \frac{\partial^2 u^*}{\partial y^{*2}} + \frac{\pi j_0 M^*}{8} e^{-\frac{\pi y^*}{a_0}}, \tag{2}$$

$$u^* \frac{\partial T^*}{\partial x^*} + v^* \frac{\partial T^*}{\partial y^*} = \frac{1}{\rho c_p} \left[\frac{\partial k(T^*)}{\partial y^*} \left(\frac{\partial T^*}{\partial y^*} \right)^2 + k(T^*) \frac{\partial^2 T^*}{\partial y^{*2}} \right] + \frac{16\sigma_{SB}}{3a_R \rho c_p} \frac{\partial}{\partial y^*} \left(T^{*3} \frac{\partial T^*}{\partial y^*} \right) + \frac{\mu(T^*)}{\rho c_p} \left(\frac{\partial u^*}{\partial y^*} \right)^2, \tag{3}$$

subject to the boundary conditions:

$$u^*(x^*, 0) = u_w^*, v^*(x^*, 0) = v_w^*, T^*(x^*, 0) = T_w^*, \tag{4}$$

$$u^*(x^*, y^* \rightarrow \infty) \rightarrow 0, T^*(x^*, y^* \rightarrow \infty) \rightarrow T_b^*. \tag{5}$$

where $\langle u^*, v^* \rangle$ represent velocity components in the direction of x^* - axis and y^* - axis respectively, T^* shows fluid temperature inside the boundary layer, $\mu(T^*) = \left(\frac{\mu_b}{1 + \mu_o(T^* - T_b^*)} \right)$ and $k(T^*) = k_b \left(1 + \varepsilon \frac{T^* - T_b^*}{T_w^* - T_b^*} \right)$ are temperature dependent viscosity and thermal conductivity of the fluid, respectively. ε is a variable thermal conductivity parameter, a_o represents the width of magnets and electrodes, M^* is the magnetization of the permanent magnets, j_o indicates the applied current density in the electrodes, σ_{SB} is the Stefan-Boltzmann constant and a_R is the Rosseland mean absorption coefficient.

Introducing the non-dimensional quantities:

$$\frac{x^*}{l} = x, \frac{y^*}{L} = y, \frac{u^*}{u_w^*} = u, \frac{v^*}{v_o} = v, \theta = \frac{T^* - T_b^*}{T_w^* - T_b^*}, \tag{6}$$

$$l = \frac{u_w^* L^2}{\vartheta_b}, L = \frac{a_o}{\pi}, v_o = \frac{\pi \vartheta_b}{a_o}, \vartheta_b = \frac{\mu_b}{\rho}, Pr = \frac{\vartheta_b \rho c_p}{k_b}, M = \frac{a_o^2 j_o M^*}{8\pi u_w^* \rho \vartheta_b} \tag{7}$$

$$Ec = \frac{u_w^{*2}}{c_p(T_w^* - T_b^*)} \text{ (Eckert number)}, Nr = \frac{a_R k_b}{4\sigma_{SB} T_b^{*3}} \text{ (thermal radiation parameter)} \tag{8}$$

into Equations (1)–(5), we have:

$$\frac{\partial u}{\partial x} + \frac{\partial v}{\partial y} = 0, \tag{9}$$

$$u \frac{\partial u}{\partial x} + v \frac{\partial u}{\partial y} = \frac{1}{1 + \delta\theta} \frac{\partial^2 u}{\partial y^2} - \frac{\delta}{(1 + \delta\theta)^2} \frac{\partial \theta}{\partial y} \frac{\partial u}{\partial y} + \frac{1}{1 + \delta\theta} \frac{\partial^2 u}{\partial y^2} + Me^{(-y)}, \tag{10}$$

$$u \frac{\partial \theta}{\partial x} + v \frac{\partial \theta}{\partial y} = \frac{1}{Pr} \left(\varepsilon \left(\frac{\partial \theta}{\partial y} \right)^2 + (1 + \varepsilon\theta) \frac{\partial^2 \theta}{\partial y^2} \right) + \frac{1}{3PrNr(\theta_r - 1)} \frac{\partial^2}{\partial y^2} (\theta(\theta_r - 1) + 1)^4 + \frac{Ec}{1 + \delta\theta} \left(\frac{\partial u}{\partial y} \right)^2, \tag{11}$$

$$u = 1, v = \frac{v_w^*}{v_o} = v_w, \theta = 1, \text{ at } y = 0, \tag{12}$$

$$u \rightarrow 0, \theta \rightarrow 0 \text{ as } y \rightarrow \infty. \tag{13}$$

By using the assumption of strong suction [6], Equations (9)–(11) can be rewritten in the following form:

$$\frac{\partial v}{\partial y} = 0, \tag{14}$$

$$v \frac{\partial u}{\partial y} = \frac{1}{1 + \delta\theta} \frac{\partial^2 u}{\partial y^2} - \frac{\delta}{(1 + \delta\theta)^2} \frac{\partial \theta}{\partial y} \frac{\partial u}{\partial y} + \frac{1}{1 + \delta\theta} \frac{\partial^2 u}{\partial y^2} + Me^{(-y)}, \tag{15}$$

$$v \frac{\partial \theta}{\partial y} = \frac{1}{Pr} \left(\varepsilon \left(\frac{\partial \theta}{\partial y} \right)^2 + (1 + \varepsilon\theta) \frac{\partial^2 \theta}{\partial y^2} \right) + \frac{1}{3PrNr(\theta_r - 1)} \frac{\partial^2}{\partial y^2} (\theta(\theta_r - 1) + 1)^4 + \frac{Ec}{1 + \delta\theta} \left(\frac{\partial u}{\partial y} \right)^2. \tag{16}$$

The condition $v = v_w$ at $y = 0$ and continuity equation gives $v = v_w$, thus Equations (15) and (16) can be written as:

$$v_w \frac{\partial u}{\partial y} = \frac{1}{1 + \delta\theta} \frac{\partial^2 u}{\partial y^2} - \frac{\delta}{(1 + \delta\theta)^2} \frac{\partial \theta}{\partial y} \frac{\partial u}{\partial y} + \frac{1}{1 + \delta\theta} \frac{\partial^2 u}{\partial y^2} + Me^{(-y)}, \tag{17}$$

$$v_w \frac{\partial \theta}{\partial y} = \frac{1}{Pr} \left(\varepsilon \left(\frac{\partial \theta}{\partial y} \right)^2 + (1 + \varepsilon\theta) \frac{\partial^2 \theta}{\partial y^2} \right) + \frac{1}{3PrNr(\theta_r - 1)} \frac{\partial^2}{\partial y^2} (\theta(\theta_r - 1) + 1)^4 + \frac{Ec}{1 + \delta\theta} \left(\frac{\partial u}{\partial y} \right)^2. \tag{18}$$

3. Entropy Generation

By assuming a viscous incompressible fluid element of a finite size such that it acts like an open thermodynamic system and by employing the second law of thermodynamics, the volumetric rate of entropy generation (\dot{E}'''_{Gen}) in the presence of non-linear Rosseland thermal radiation and viscous dissipation takes the following form:

$$\dot{E}'''_{Gen} = \frac{k(T^*)}{T^{*2}} \left(\frac{\partial T^*}{\partial y^*} \right)^2 + \frac{\mu(T^*)}{T^*} \left(\frac{\partial u^*}{\partial y^*} \right)^2 + k(T^*) \frac{16\sigma_{SB}T^*}{3a_R k(T^*)} \left(\frac{\partial T^*}{\partial y^*} \right)^2 \tag{19}$$

Using the transformations defined in Equations (6)–(8) we obtained the dimensionless form of volumetric rate of entropy generation Ns as given below

$$Ns = \frac{\dot{E}'''_{Gen}}{(\dot{E}'''_{Gen})_o} = (\theta_r - 1)^2 \underbrace{\left[\frac{1 + \varepsilon\theta}{(\theta(\theta_r - 1) + 1)^2} + \frac{4}{3Nr} (\theta(\theta_r - 1) + 1) \right]}_{\text{Thermal irreversibility}} \left(\frac{\partial \theta}{\partial y} \right)^2 + \underbrace{\frac{EcPr(\theta_r - 1)}{(1 + \delta\theta)(\theta(\theta_r - 1) + 1)} \left(\frac{\partial u}{\partial y} \right)^2}_{\text{Frictional irreversibility}} \tag{20}$$

here $(\dot{E}'''_{Gen})_o = \frac{k_b}{L^2}$ is the characteristic entropy generation, $\theta_r = \frac{T_w^*}{T_b^*}$ denotes the heating parameter, $\delta = \mu_o(T_w^* - T_b^*)$ indicates a parameter related to variable viscosity.

4. Results and Discussion

The numerical solutions of the system of Equations (17) and (18) with the corresponding boundary conditions (12, 13) are obtained using Matlab in-built boundary value solver bvp4c. The numerical values of $\left(\frac{\partial \theta}{\partial y} \right)_{y=0}$ are tabulated in Table 1. This table shows that the numerical values obtained by using bvp4c and shooting method are sufficiently close to each other, which validates our current numerical procedure. The obtained numerical solutions are used to examine the behavior of entropy generation against the various embedding physical parameters. Figure 2a shows the variations in velocity profile for different values of the modified Hartmann number M . Here we observed that velocity of the fluid $u(y)$ accelerates with an increase in modified Hartmann number. This is consistent with the physics of the problem because $M > 0$ implies adding flow mechanism on the velocity profile. Figure 2b reflects the variation of temperature profile with increasing modified Hartmann number. It is revealed that an increase occurs in the temperature profile with rising values of modified Hartmann number. The variations in entropy generation corresponding to different values of the modified Hartmann number is shown in Figure 2c. A reduction in entropy generation is noticed with the enhancement of a modified Hartmann number. Whereas this behavior is reversed after a certain vertical distance from a Riga plate. Figure 3a elaborates the effects of the mass suction parameter v_w on $u(y)$. The decrease in

fluid velocity is observed with increasing mass suction parameter. Physically, suction pulls the fluid towards the surface of the Riga plate and this pulling acts as a retarding force, consequently, velocity decays. Further, the thickness of the viscous boundary layer decays with the increasing mass suction parameter v_w . The ability of mass suction parameter v_w to reduce the thermal boundary layer is clearly seen from Figure 3b. In addition, the temperature also decays and asymptotically approaches to zero towards the edge of the temperature boundary layer. The enhancement in the entropy generation with increasing mass suction parameter v_w is shown in Figure 3c. Physically, this is because of increasing thermal and velocity gradients with increasing mass suction parameter. Figure 4a demonstrates the variations of temperature $\theta(y)$ against the rising values of the heating parameter θ_r . It is noticed that temperature $\theta(y)$ rises with the increasing values of θ_r . The increasing behavior of temperature is expected because θ_r increases with increasing the operating temperature difference $T_w^* - T_b^*$ and consequently the fluid temperature rises. It is noticed from Figure 4b that the increase in heating parameter enhances the entropy generation. The heating of fluid due to increased heating parameter causes more entropy generation. Further, the effects are significant at the surface of Riga plate and its proximity. Figure 5a presented the influence of variable viscosity parameter δ on the velocity profile $u(y)$. It is found that $u(y)$ decays with variable viscosity parameter δ . The influence of δ on entropy generation number N_s is depicted in Figure 5b. The entropy generation increase with the rising values of δ . This is due to the increasing velocity gradients with the increasing values of δ . The enhancement in entropy generation is prominent at the surface and near the surface of the Riga plate. Additionally, maximum entropy generation is observed at the surface of the Riga plate. The increasing trend of N_s is reversed after a certain distance y . Figure 6a presents the variations in temperature $\theta(y)$ corresponding to increasing values of Prandtl number Pr. The influence of Pr is to decrease the fluid temperature. Physically, with growing values of Pr the thermal diffusivity reduces which is responsible for the decay of temperature profile. Figure 6b presents the distribution of entropy generation for against the multiple values of the Prandtl number. It is clearly seen that N_s enhances if Pr increases. Physically, the thermal gradients increase with growing values of Pr and so the entropy generation increases.

Table 1. Comparison of the numerical values of $\left(\frac{\partial \theta}{\partial y}\right)_{y=0}$ for different embedding physical flow parameters.

								$\left(\frac{\partial \theta}{\partial y}\right)_{y=0}$	
v_w	M	δ	ε	Pr	Ec	N_r	θ_r	Shooting	bvp4c
-3.0	2.5	0.2	0.3	1.2	0.5	1.0	1.2	-0.93626	-0.93625
-4.0								-1.23309	-1.23310
-5.0								-1.51387	-1.51385
-3.0	1.0							-0.85674	-0.85672
	2.0							-0.92065	-0.92065
	3.0							-0.94096	-0.94097
	2.5	0.0						-0.93125	-0.93125
		0.5						-0.94241	-0.94242
		1.0						-0.95012	-0.95010
		0.3	0.0					-1.02348	-1.02350
			0.5					-0.88924	-0.88925
			1.0					-0.78617	-0.78616
			0.3	0.7				-0.54823	-0.54825
				1.2				-0.93847	-0.93847
				3.0				-2.33939	-2.33938
				1.2	0.0			-0.99889	-0.99890
					0.3			-0.96259	-0.96257
					0.6			-0.92643	-0.92645
					0.5			-0.93847	-0.93845
						1.0		-1.37779	-1.37780
						5.0		-1.91672	-1.91671
						1.0	1.1	-1.09966	-1.09967
							1.2	-0.93847	-0.93846
							1.3	-0.79999	-0.79999

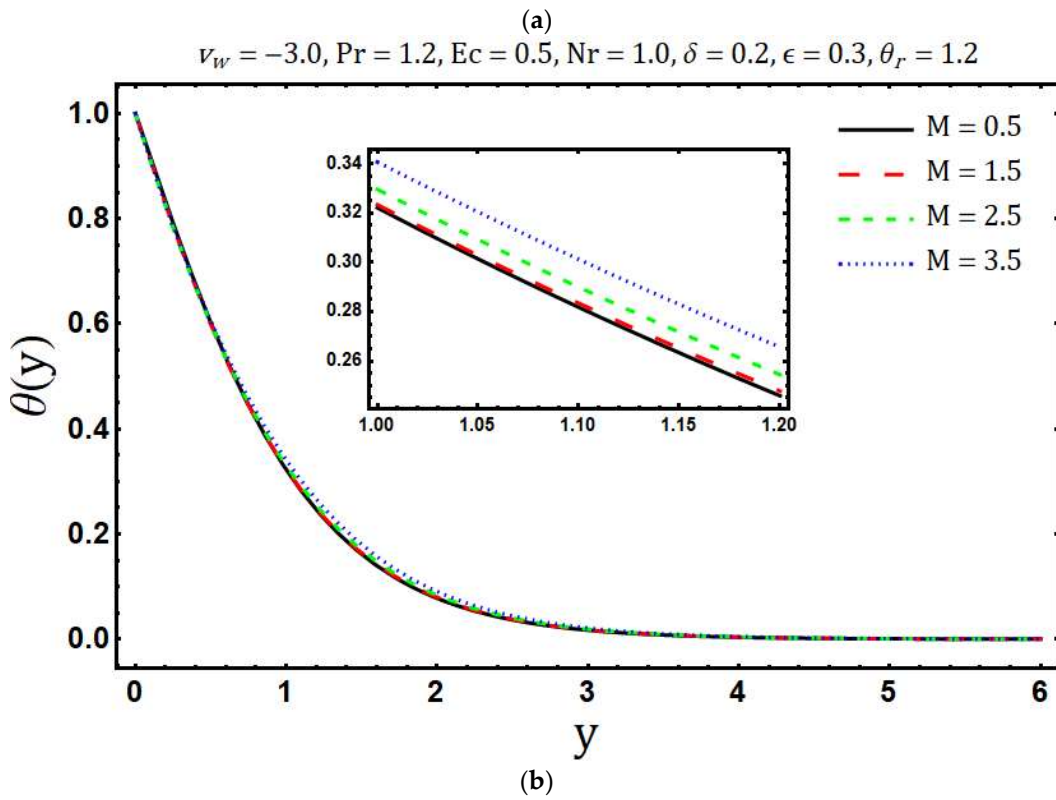
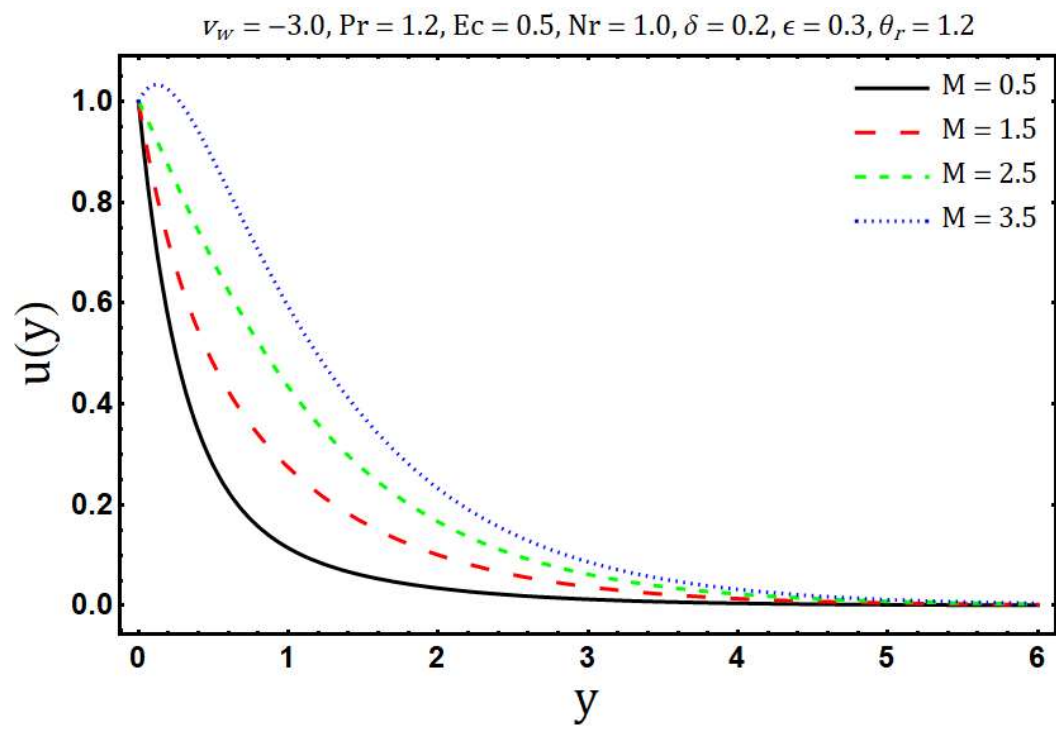


Figure 2. Cont.

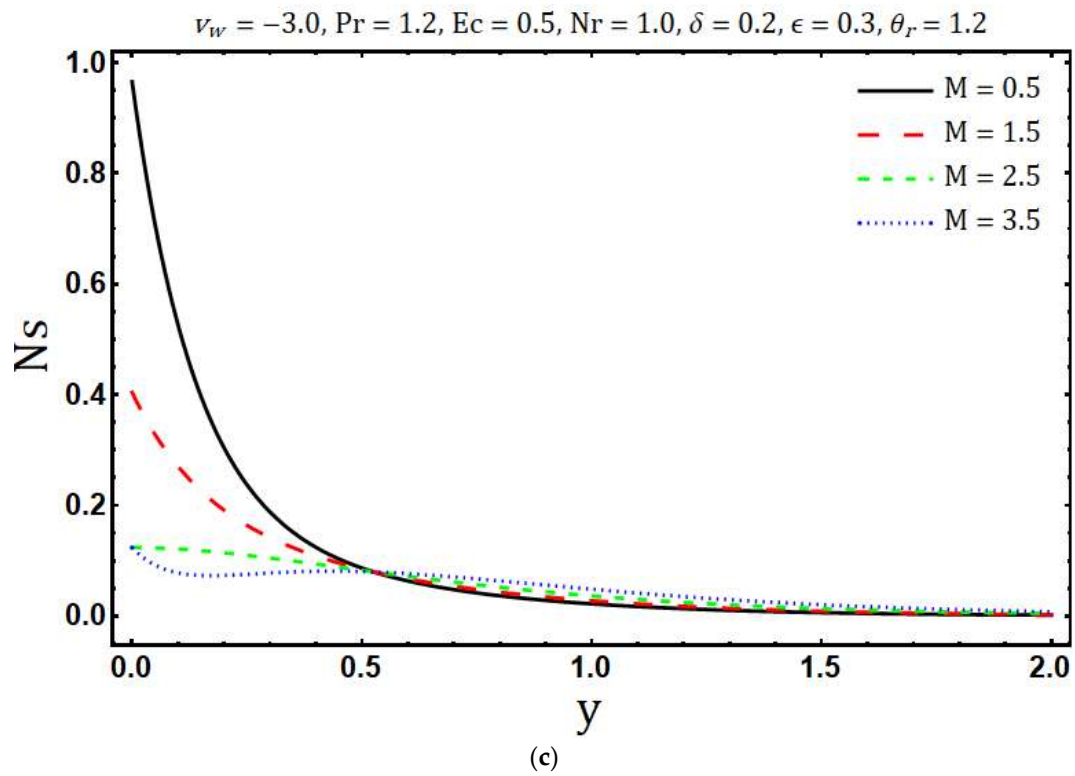


Figure 2. Effects of M on (a) velocity profile (b) temperature distribution and (c) entropy generation.

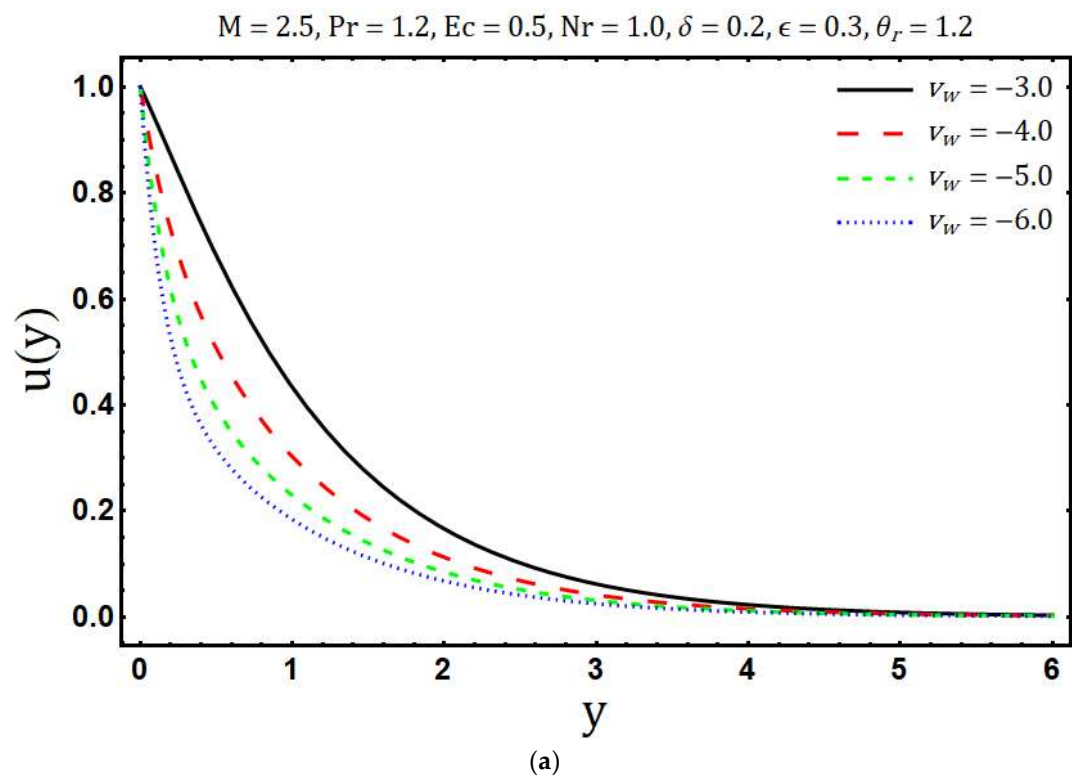


Figure 3. Cont.

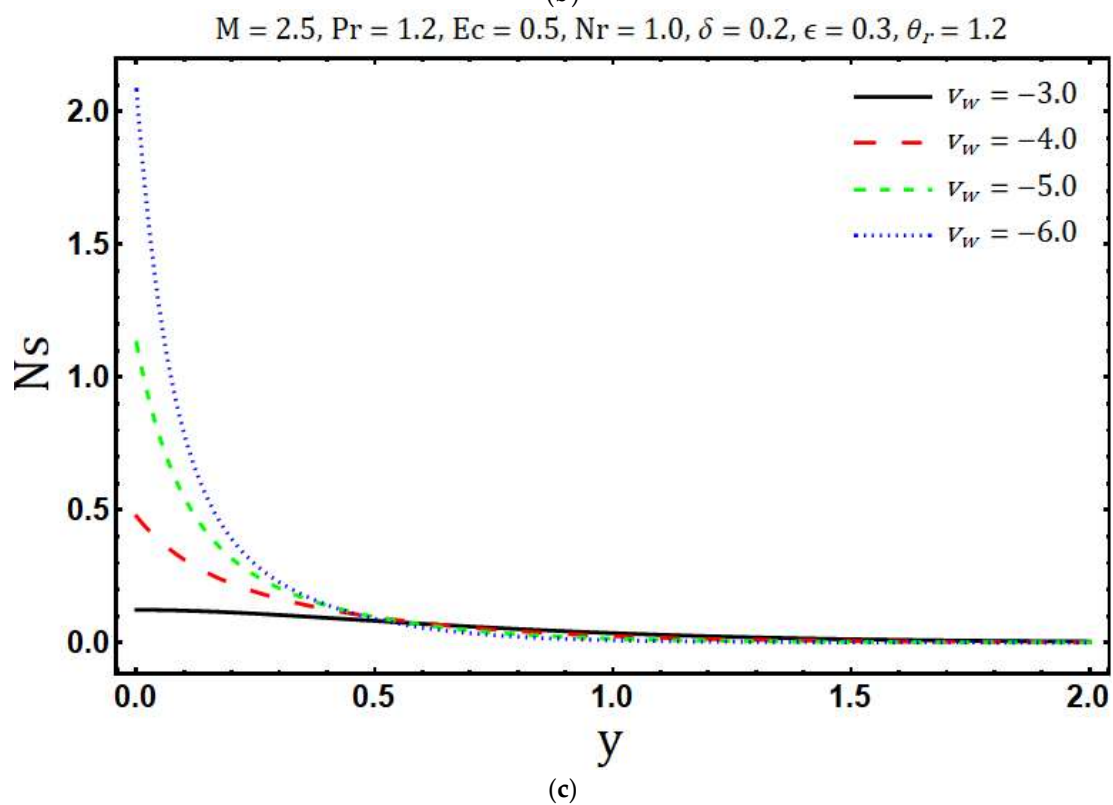
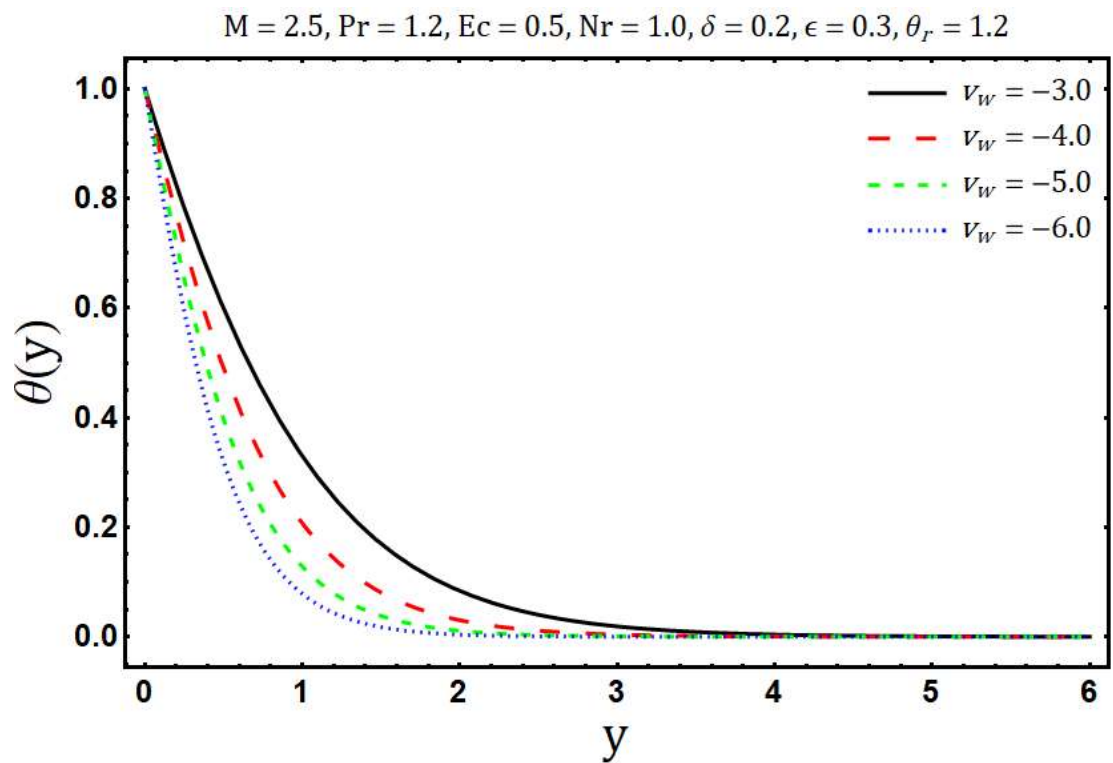


Figure 3. Effects of v_w on (a) velocity profile (b) temperature distribution and (c) entropy generation.

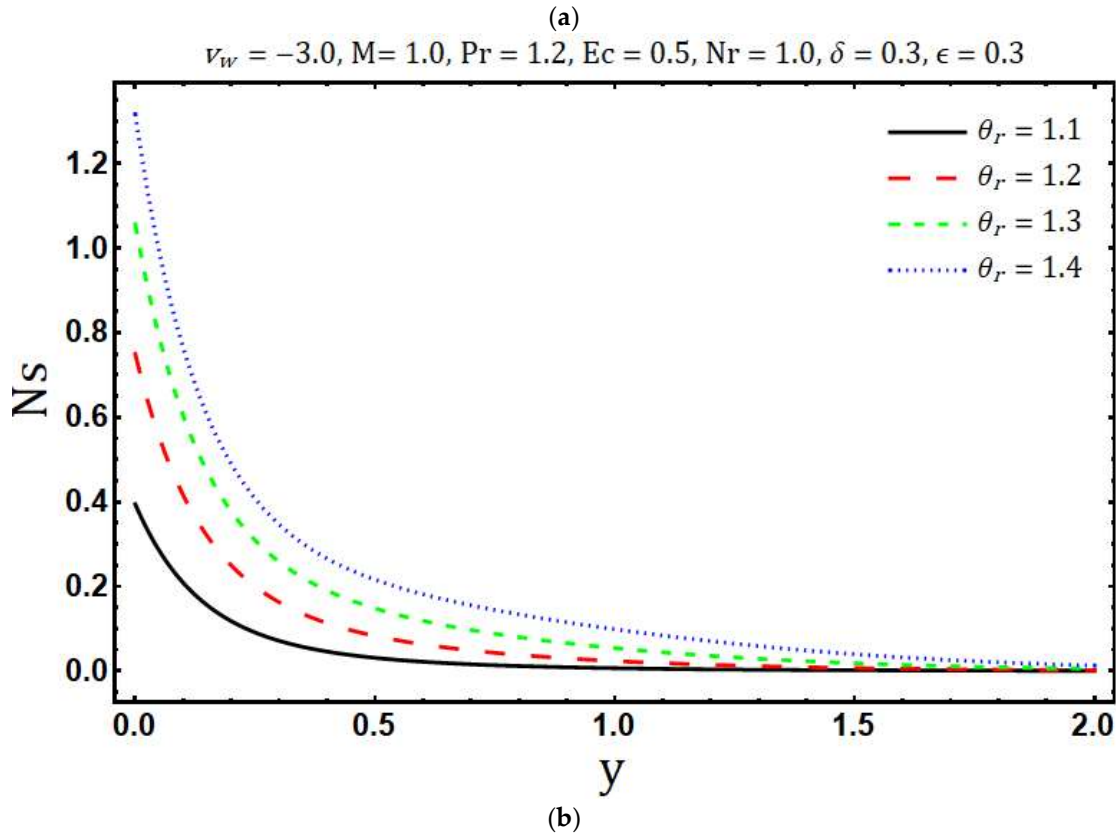
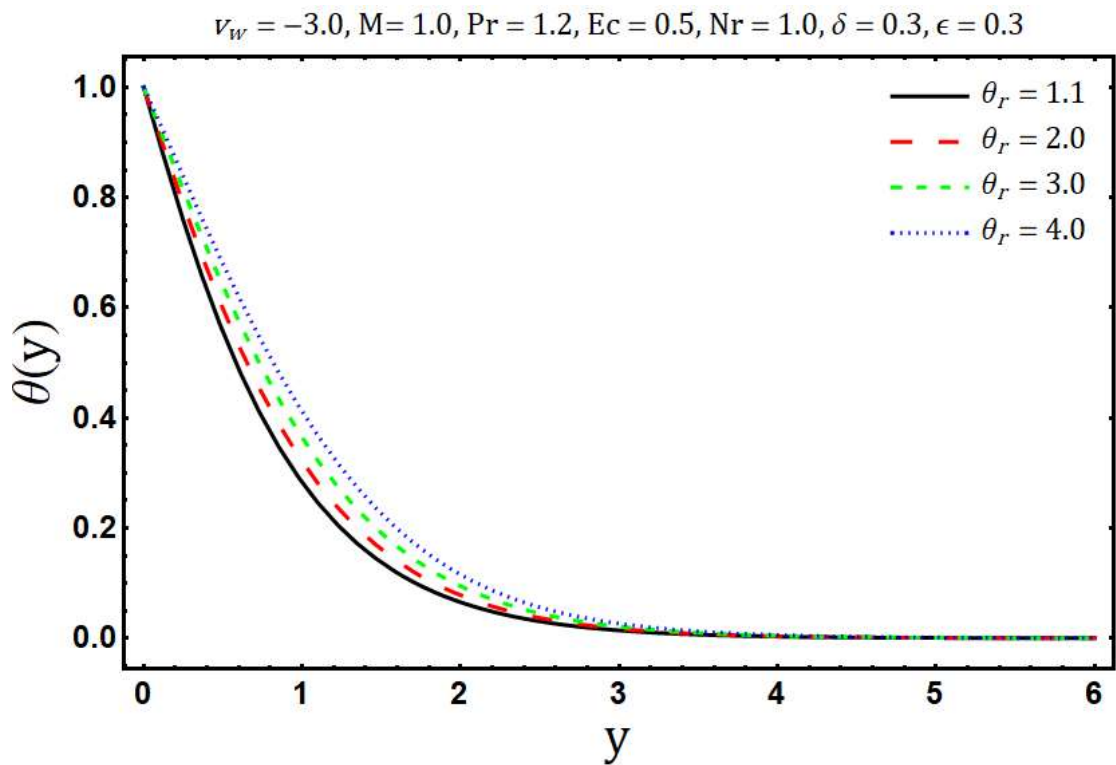


Figure 4. Effects of θ_r on (a) temperature distribution and (b) entropy generation.

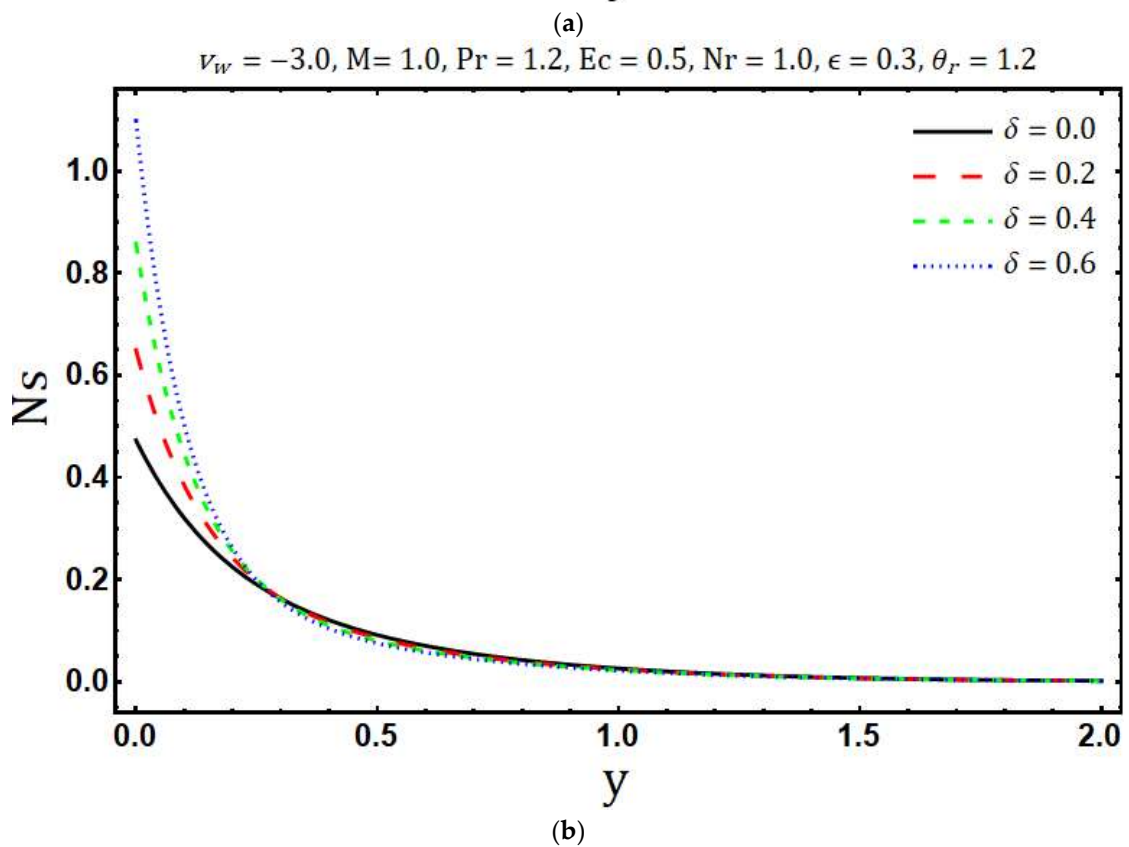
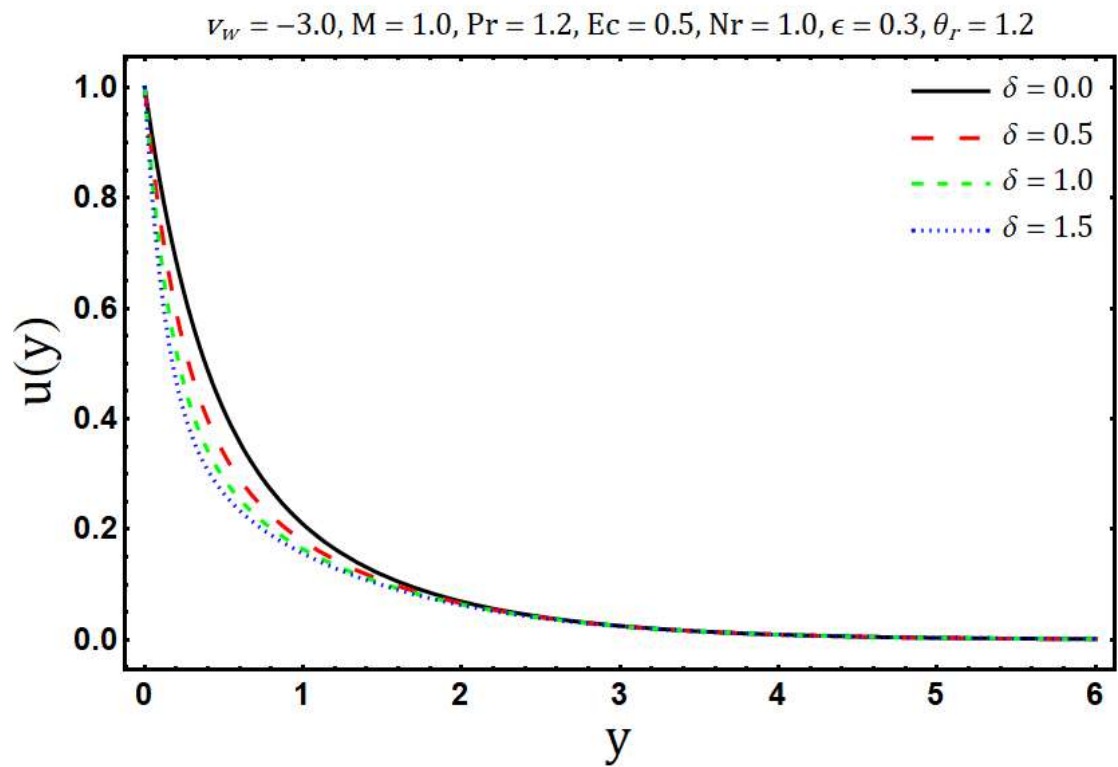


Figure 5. Effects of δ on (a) velocity profile and (b) entropy generation.

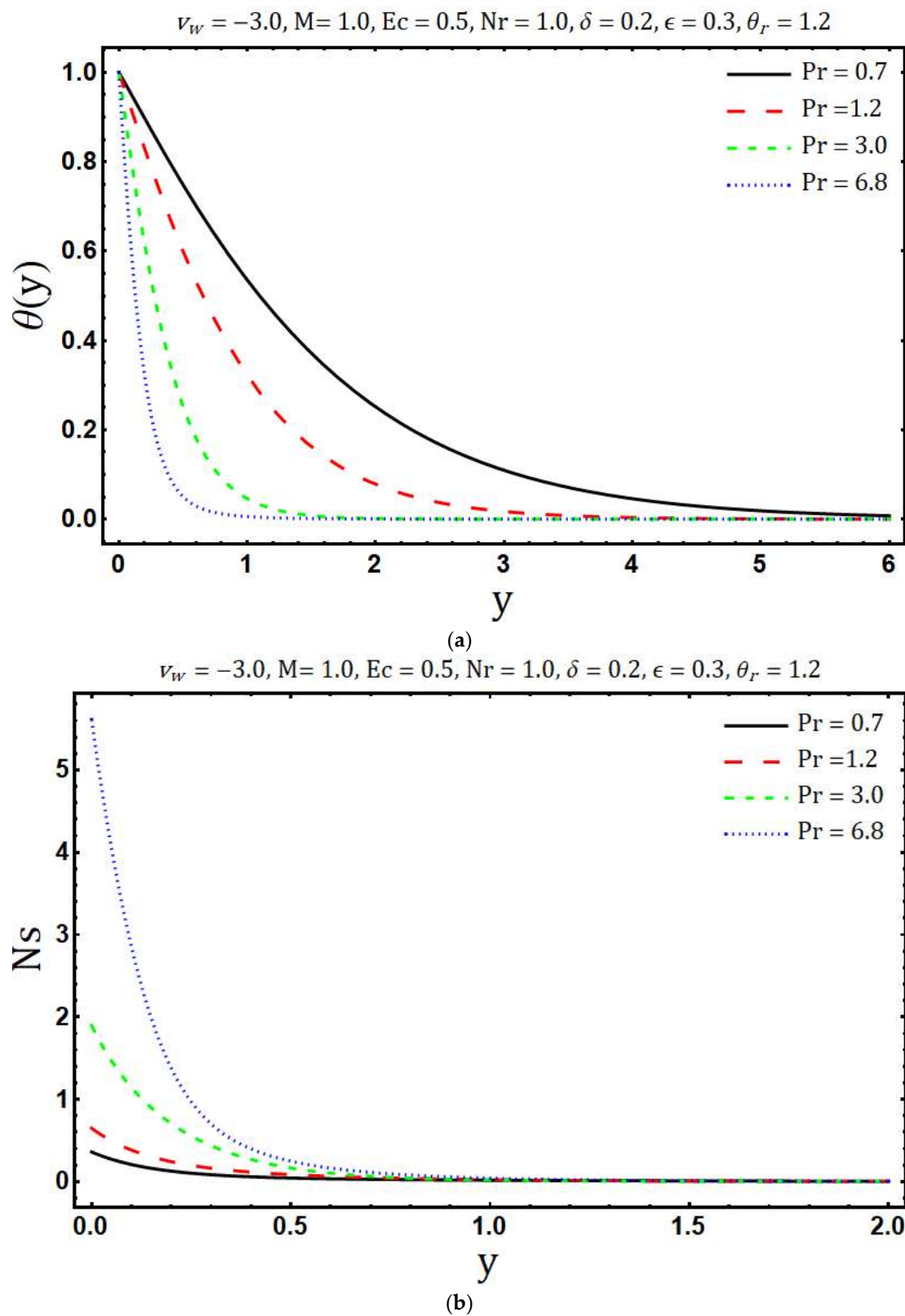


Figure 6. Effects of Pr on (a) temperature distribution and (b) entropy generation.

Figure 7a portrays the effects of variable thermal conductivity parameter ϵ on temperature $\theta(y)$. It is found that the temperature $\theta(y)$ and thickness of the thermal boundary layer increase if ϵ increases.

This is due to the fact that thermal conductivity increases with growing values of ϵ which in turn enhances the thermal energy penetration. The influence of ϵ on the entropy generation is shown in Figure 7b. The ϵ tends to decrease the entropy generation and this is because of the decreasing thermal gradients with rising values of ϵ . Impacts of thermal radiation parameter N_r on temperature $\theta(y)$ are presented in Figure 8a. It is found that as the values of N_r increases, $\theta(y)$ decreases. Physically, for a given value of k_b and a_R , an increase in $N_r = \frac{k_b a_R}{4\sigma_{SB} T_b^3}$ yields a decrease in the ambient temperature T_b^* and this means that significant part of the fluid inside the boundary layer has low temperature and consequently the thermal diffusivity $\left(\alpha + \frac{16\sigma_{SB}}{3\rho c_p a_R} T^3\right)$ becomes low with the thin thermal boundary layer. The effect of N_r on distribution of entropy generation in the main flow region is depicted in Figure 8b. It is clearly seen that Ns enhances with growing values of N_r whereas opposite trend is observed after a certain transverse distance y . Further, the surface of the Riga plate is the strong source of entropy generation due to the large thermal and velocity gradients. In Figure 9a temperature $\theta(y)$ is plotted against the transversal distance y for different values of the Eckert number Ec . The increase in $\theta(y)$ is observed with the increasing values of Ec and this is because of dissipative frictional forces between the fluid layer. The influence of different increasing values of Ec on Ns is illustrated in Figure 9b. It is found that an increase in the Ec leads to enhance the Ns . Physically, the dissipative frictional forces between the fluid layer increase with increasing Eckert number and consequently entropy generation enhances.

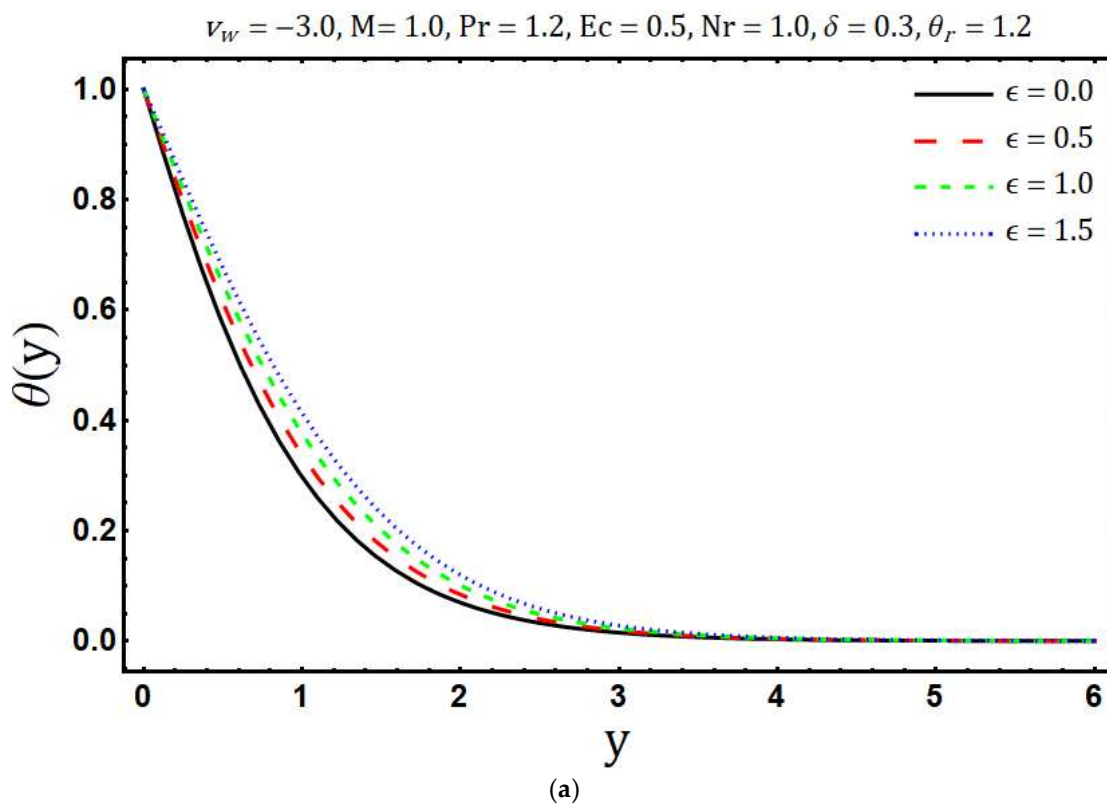


Figure 7. Cont.

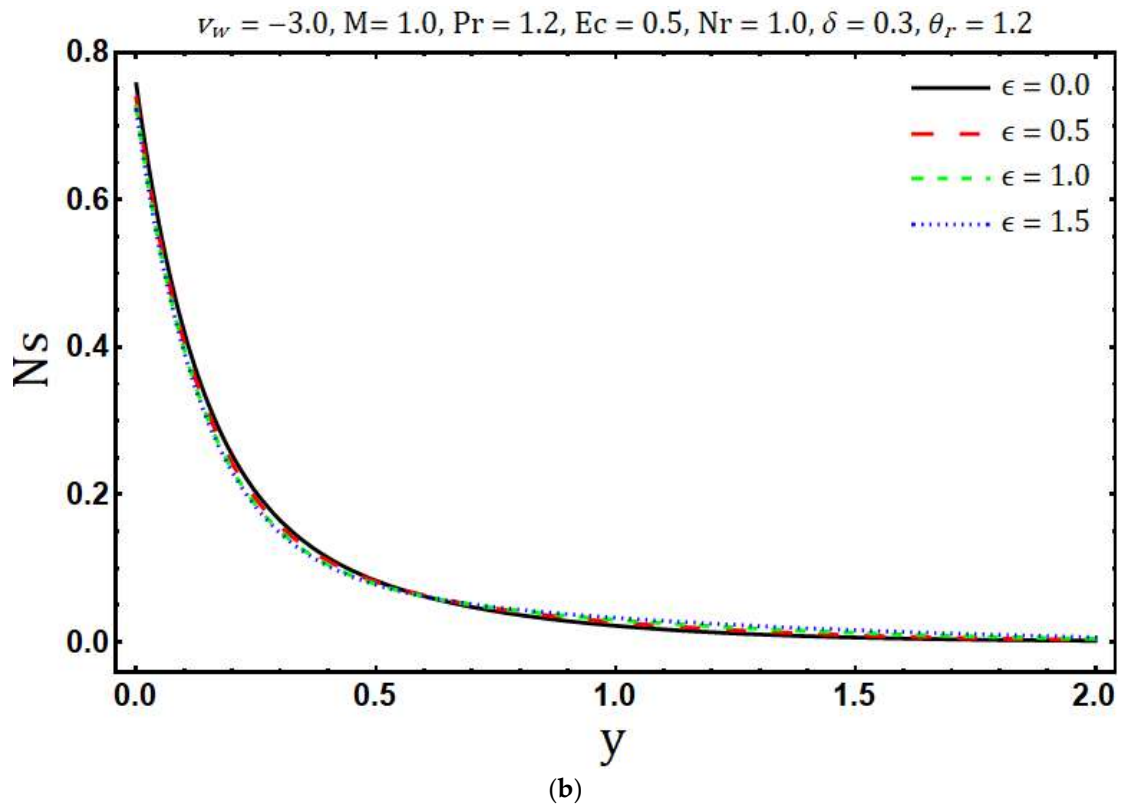


Figure 7. Effects of ϵ on (a) temperature distribution and (b) entropy generation.

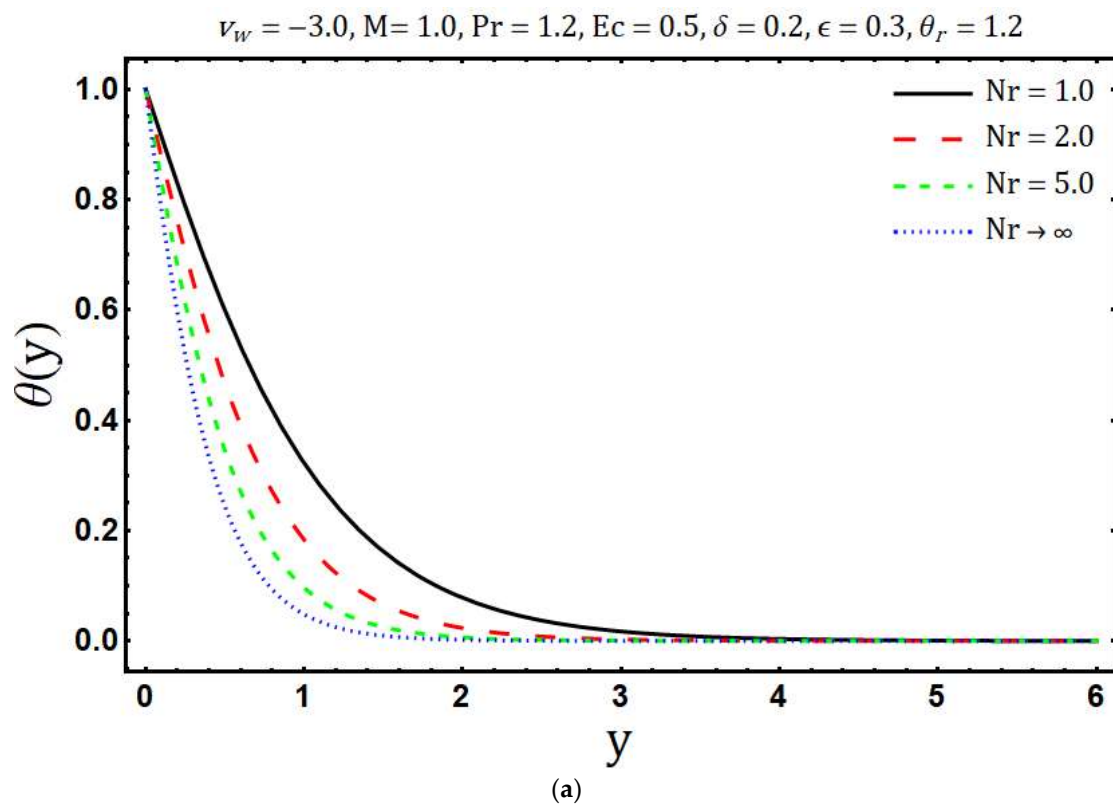


Figure 8. Cont.

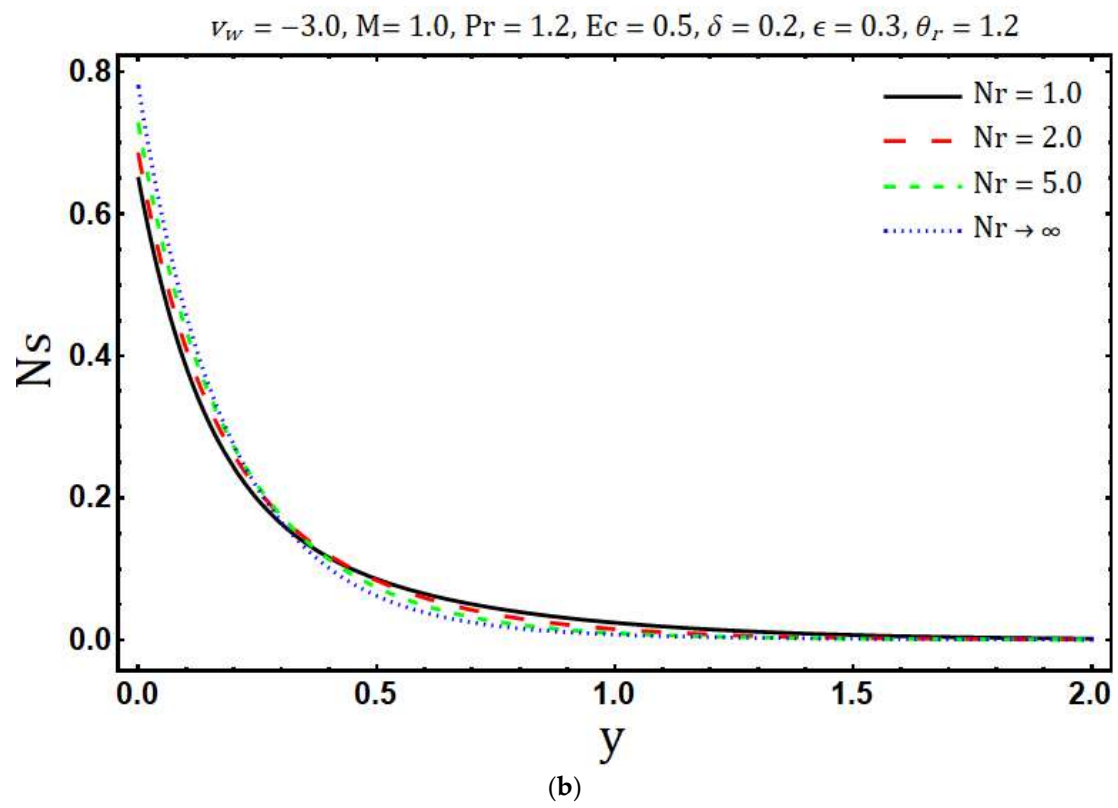


Figure 8. Effects of N_r on (a) temperature distribution and (b) entropy generation.

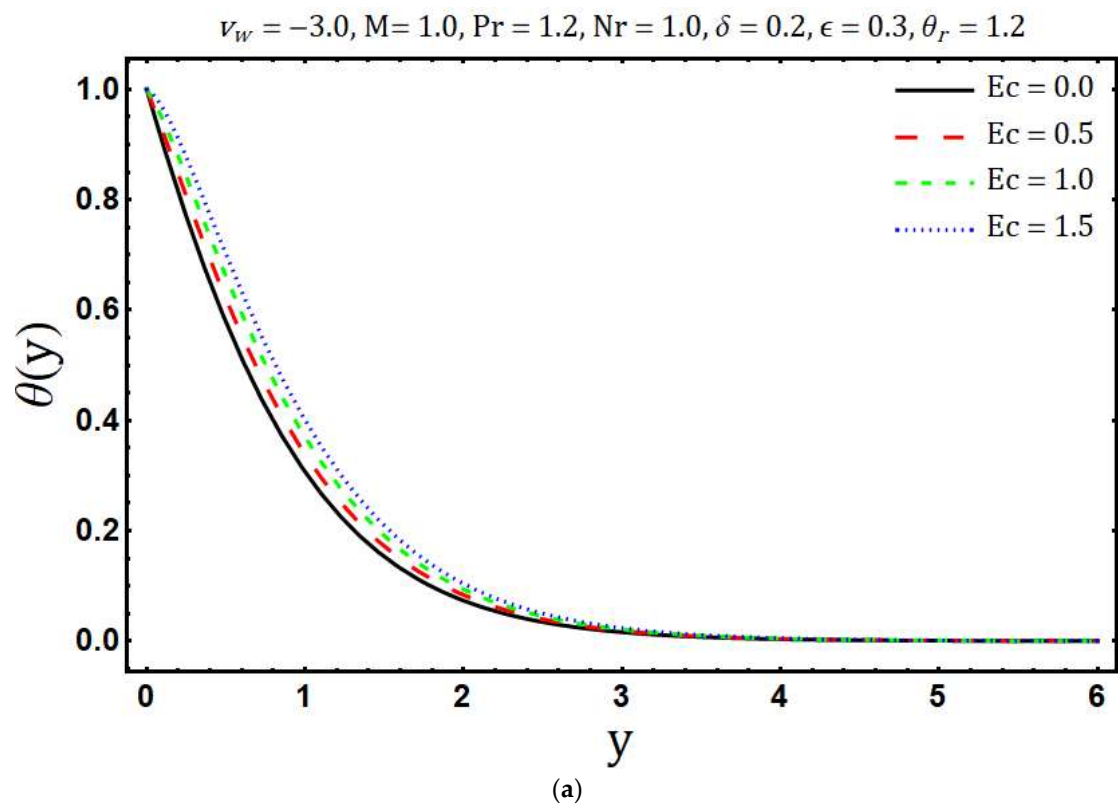


Figure 9. Cont.

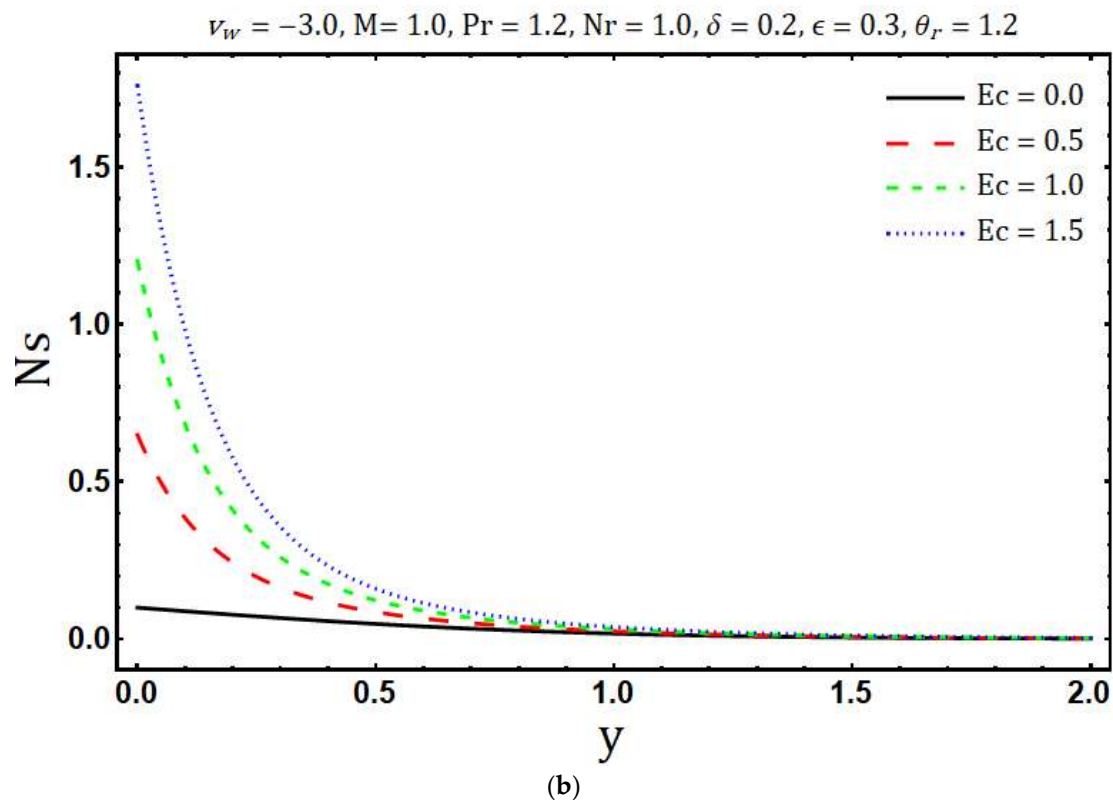


Figure 9. Effects of Ec on (a) temperature distribution and (b) entropy generation.

5. Concluding Remarks

Numerical computation has been done to examine the heat transfer and entropy generation in boundary layer flow over a Riga plate by considering the effects of non-linear thermal radiation with variable transport properties. The following are the main outcomes drawn from this study:

- Decay in the magnitude of velocity $u(y)$ is found as the mass suction parameter v_w and variable viscosity parameter increases δ while an enhancement in modified Hartmann number M accelerates the fluid motion.
- Temperature $\theta(y)$ increases with rising values of the Eckert number, heating parameter, and variable thermal conductivity while an opposite behavior has been observed for growing values of the mass suction parameter, Prandtl number, and radiation parameter N_r .
- The decrement in entropy generation Ns is observed with increasing values of modified Hartmann number and variable thermal conductivity while increment in Ns is observed with rising values of Prandtl number, radiation parameter, mass suction parameter, Eckert number, variable viscosity parameter and heating parameter.
- Maximum entropy is generated at the surface of Riga plate.

Author Contributions: Muhammad Idrees Afridi and Muhammad Qasim formulated the problem. Muhammad Qasim solved the problem. Muhammad Idrees Afridi and Abid Hussanan computed and analyzed the results. All the authors equally contributed in writing and proof reading of the paper.

Funding: This research received no external funding. The APC was given by Ton Duc Thang University, Ho Chi Minh City, Vietnam. However, no grant number is available from source.

Acknowledgments: The corresponding author would like to acknowledge Ton Duc Thang University, Ho Chi Minh City, Vietnam for the financial support.

Conflicts of Interest: The authors declare no conflict of interest.

Nomenclature

a_o	with of electrodes and magnets (m)
c_p	specific heat at constant pressure (J/kg K)
Ec	Eckert number
\dot{E}_{Gen}'''	volumetric rate of entropy generation (W/K)
$(\dot{E}_{Gen}''')_o$	characteristic volumetric rate of entropy generation (W/K)
j_o	current density (A/m^2)
$k(T^*)$	temperature dependent thermal conductivity (W/mK)
k_b	thermal conductivity of fluid outside the boundary layer (W/mK)
L	length unit (m)
M^*	magnetization of the magnets (Tesla)
M	modified Hartmann number
N_r	thermal radiation parameter
N_s	entropy generation number
Pr	Prandtl number
T^*	fluid temperature (K)
T_w^*	temperature at the surface of Riga-plate (K)
T_b^*	ambient temperature (K)
u^*	horizontal velocity (ms^{-1})
u	dimensionless horizontal velocity
v^*	vertical component of velocity (ms^{-1})
v	dimensionless vertical velocity
x^*	horizontal coordinate (m)
x	dimensionless horizontal coordinate
y^*	vertical coordinate (m)
y	dimensionless vertical coordinate

Greek Symbols

ε	variable thermal conductivity parameter
δ	variable viscosity parameter
$\mu(T^*)$	dynamic viscosity (kg/ms)
μ_b	dynamic viscosity of ambient fluid (kg/ms)
ϑ_b	kinematic viscosity of ambient fluid (m^2/s)
ρ	fluid density (kg/m^3)
θ	dimensionless temperature
θ_r	heating parameter

Subscripts

w	condition on boundary
b	condition outside the boundary layer

References

1. Gailitis, A.; Lielausis, O. On a possibility to reduce the hydrodynamic resistance of a plate in an electrolyte. *Appl. Magneto hydrodyn. Rep. Phys. Inst. Riga* **1961**, *12*, 143–146.
2. Avilov, V.V. *Electric and Magnetic Fields for the Riga Plate*; Technical Report; FRZ: Rossendorf, Germany, 1998.
3. Tsinober, A.B.; Shtern, A.G. Possibility of increasing the flow stability in a boundary layer by means of crossed electric and magnetic fields. *Magneto hydrodynamics* **1967**, *3*, 103–105.
4. Pantokratoras, A. The Blasius and Sakiadis flow along a Riga-plate. *Prog. Comput. Fluid Dyn.* **2011**, *11*, 329–333. [[CrossRef](#)]
5. Magyari, E.; Pantokratoras, A. Aiding and opposing mixed convection flows over the Riga-plate. *Commun. Nonlinear Sci. Numer. Simul.* **2011**, *16*, 3158–3167. [[CrossRef](#)]
6. Ahmad, A.; Asghar, S.; Afzal, S. Flow of nanofluid past a Riga plate. *J. Magn. Magn. Mater.* **2016**, *402*, 44–48. [[CrossRef](#)]

7. Ramesh, G.K.; Gireesha, B.J. Non-linear radiative flow of nanofluid past a moving/stationary Riga plate. *Front. Heat Mass Transf.* **2017**, *9*, 1–7. [[CrossRef](#)]
8. Pantokratoras, A.; Magyari, E. EMHD free-convection boundary-layer flow from a Riga-plate. *J. Eng. Math.* **2009**, *64*, 303–315. [[CrossRef](#)]
9. Pantokratoras, A.; Fang, T. Sakiadis flow with nonlinear Rosseland thermal radiation. *Phys. Scr.* **2012**, *87*, 015703. [[CrossRef](#)]
10. Pantokratoras, A.; Fang, T. Blasius flow with nonlinear Rosseland thermal radiation. *Meccanica* **2014**, *49*, 1539–1545. [[CrossRef](#)]
11. Afridi, M.I.; Qasim, M. Entropy generation and heat transfer in boundary layer flow over a thin needle moving in a parallel stream in the presence of nonlinear Rosseland radiation. *Int. J. Therm. Sci.* **2018**, *123*, 117–128. [[CrossRef](#)]
12. Sithole, H.; Mondal, H.; Sibanda, P. Entropy generation in a second grade magnetohydrodynamic nanofluid flow over a convectively heated stretching sheet with nonlinear thermal radiation and viscous dissipation. *Res. Phys.* **2018**, *9*, 1077–1085. [[CrossRef](#)]
13. Babu, M.J.; Sandeep, N. Effect of nonlinear thermal radiation on non-aligned bio-convective stagnation point flow of a magnetic-nanofluid over a stretching sheet. *Alex. Eng. J.* **2016**, *55*, 1931–1939. [[CrossRef](#)]
14. Ghadikolaei, S.S.; Hosseinzadeh, K.; Ganji, D.D.; Jafari, B. Nonlinear thermal radiation effect on magneto Casson nanofluid flow with Joule heating effect over an inclined porous stretching sheet. *Case Stud. Therm. Eng.* **2018**, *12*, 176–187. [[CrossRef](#)]
15. Hossain, M.A.A.; Munir, M.S. Mixed convection flow from a vertical flat plate with temperature dependent viscosity. *Int. J. Therm. Sci.* **2000**, *39*, 173–183. [[CrossRef](#)]
16. Khader, M.M.; Megahed, A.M. Approximate solutions for the flow and heat transfer due to a stretching sheet embedded in a porous medium with variable thickness, variable thermal conductivity and thermal radiation using Laguerre collocation method. *Appl. Appl. Math. Int. J.* **2015**, *10*, 817–834.
17. Mureithi, E.W.; Mwaonanyi, J.J.; Makinde, O.D. On the boundary layer flow over a moving surface in a fluid with temperature-dependent viscosity. *Open J. Fluid Dyn.* **2013**, *3*, 135–140. [[CrossRef](#)]
18. Pal, D.; Mondal, H. Effects of temperature-dependent viscosity and variable thermal conductivity on MHD non-Darcy mixed convective diffusion of species over a stretching sheet. *J. Egypt. Math. Soc.* **2014**, *22*, 123–133. [[CrossRef](#)]
19. Manjunatha, S.; Gireesha, B.J. Effects of variable viscosity and thermal conductivity on MHD flow and heat transfer of a dusty fluid. *Ain Shams Eng. J.* **2016**, *7*, 505–515. [[CrossRef](#)]
20. Lin, Y.; Zheng, L.; Zhang, X. Radiation effects on Marangoni convection flow and heat transfer in pseudo-plastic non-Newtonian nanofluids with variable thermal conductivity. *Int. J. Heat Mass Transf.* **2014**, *77*, 708–716. [[CrossRef](#)]
21. Hsiao, K.L. To Promote radiation electrical MHD activation Energy Thermal Extrusion Manufacturing System Efficiency by Using Carreau-Nanofluid with Parameters Control Method. *Energy* **2017**, *130*, 486–499. [[CrossRef](#)]
22. Lin, Y.; Zheng, L.; Li, B.; Ma, L. A new diffusion for laminar boundary layer flow of power law fluids past a flat surface with magnetic effect and suction or injection. *Int. J. Heat Mass Transf.* **2015**, *90*, 1090–1097. [[CrossRef](#)]
23. Olatundun, A.T.; Makinde, O.D. Analysis of Blasius flow of hybrid nanofluids over a convectively heated surface. *Defect Diffus. Forum* **2017**, *377*, 29–41. [[CrossRef](#)]
24. Hsiao, K.L. Stagnation Electrical MHD Nanofluid Mixed Convection with Slip Boundary on a Stretching Sheet. *Appl. Therm. Eng.* **2016**, *98*, 850–861. [[CrossRef](#)]
25. Seini, I.Y.; Makinde, O.D. Boundary layer flow near stagnation-points on a vertical surface with slip in the presence of transverse magnetic field. *Int. J. Numer. Methods Heat Fluid Flow* **2014**, *24*, 643–653. [[CrossRef](#)]
26. Bejan, A. *Entropy Generation Minimization*; CRC Press: New York, NY, USA, 1996.
27. Bejan, A. The thermodynamic design of heat and mass transfer processes and devices. *Heat Fluid Flow* **1987**, *8*, 258–276. [[CrossRef](#)]
28. Afridi, M.I.; Qasim, M.; Khan, I.; Shafie, S.; Alshomrani, A.S. Entropy generation in Magnetohydrodynamic mixed convection flow over an inclined stretching sheet. *Entropy* **2017**, *19*, 10. [[CrossRef](#)]
29. Rashidi, M.M.; Freidoonimehr, N. Analysis of entropy generation in MHD stagnation-point flow in porous media with heat transfer. *Int. J. Comput. Methods Eng. Sci. Mech.* **2014**, *15*, 345–355. [[CrossRef](#)]

30. Afridi, M.I.; Qasim, M. Entropy generation in three-dimensional flow of dissipative fluid. *Int. J. Appl. Comput. Math.* **2018**, *16*, 16. [[CrossRef](#)]
31. Chamkha, A.J.; Ismael, M.; Kasaeipour, A.; Armaghani, T. Entropy generation and natural convection of CuO-Water nanofluid in C-shaped cavity under magnetic field. *Entropy* **2016**, *18*, 50. [[CrossRef](#)]
32. Das, S.; Jana, R.N.; Chamkha, A.J. Entropy generation due to unsteady hydromagnetic Couette flow and heat transfer with asymmetric convective cooling in a rotating system. *J. Math. Model.* **2015**, *3*, 107–128.
33. Butt, A.S.; Ali, A.; Tufail, N.; Mehmood, A. Entropy production in mixed convective magnetohydrodynamic flow of nanofluid over a linearly stretching sheet. *J. Nanofluids* **2017**, *6*, 379–389. [[CrossRef](#)]
34. Afridi, M.I.; Qasim, M.; Shafie, S. Entropy generation in hydromagnetic boundary flow under the effects of frictional and Joule heating: Exact solutions. *Eur. Phys. J. Plus* **2017**, *132*, 3–11. [[CrossRef](#)]
35. Butt, A.S.; Ali, A. Entropy analysis of magnetohydrodynamic flow and heat transfer due to stretching cylinder. *J. Taiwan Inst. Chem. Eng.* **2014**, *45*, 780–786. [[CrossRef](#)]



© 2018 by the authors. Licensee MDPI, Basel, Switzerland. This article is an open access article distributed under the terms and conditions of the Creative Commons Attribution (CC BY) license (<http://creativecommons.org/licenses/by/4.0/>).